Vapor−Liquid and Vapor−Liquid−Liquid Equilibria of Carbon Dioxide/*n*-Perfluoroalkane/*n*-Alkane Ternary Mixtures

Coray M. Colina and Keith E. Gubbins*

Department of Chemical and Biomolecular Engineering, North Carolina State University, Raleigh, North Carolina 27695

Received: July 29, 2004; In Final Form: November 18, 2004

Perfluoroalkanes have numerous applications (e.g., in the medical field and the chemical industry), and their high affinity for carbon dioxide makes them attractive as surfactants and cosolvents. Although research in this area has grown in the past few years, very little phase-equilibrium data is available in the open literature for these systems. In this work, we present, for the first time, predictions of vapor−liquid and vapor−liquid−liquid equilibria of binary and ternary systems of carbon dioxide/*n*-perfluoroalkane/*n*-alkane. Our results are based on the SAFT-VR EOS (statistical associating fluid theory of variable range, equation of state), and we study the influence of temperature, pressure, composition, and chain length on the phase diagram. The predicted phase diagrams are based on temperature-*in*dependent binary interaction parameters, and *no* ternary parameters are introduced. Comparisons to the available experimental and molecular simulation data show that the predicted diagrams should provide a good representation of the phase equilibria.

Introduction

Perfluoroalkanes have been used in the medical field and the chemical industry in numerous applications. Liquid ventilation is a novel life-support technique in which the lungs are partially or totally filled with a neat liquid perfluorocarbon that acts as the oxygen and carbon dioxide carrier.[1,2] Perfluorooctylbromide ($C_8F_{17}Br$) is undergoing Food and Drug Administration phase II and III clinical evaluation, and several other (liquid) perfluorocarbons, including perfluorooctane (n-C_8F_{18}), are currently under investigation.[2] Moreover, these fluids have been suggested as a vehicle for drug delivery[2] because of their higher solubility for oxygen and carbon dioxide and lower surface tension than that of water. Additionally, their resemblance to inhaled anesthetic agents suggests the possibility of their application in vaporization,[1] a new medical technique that has significantly improved oxygenation and pulmonary function in oleic acid-induced lung injury. Perfluorohexane (n-C_6F_{14}) has been used to investigate[1] its effects on gas exchange and lung function in an ovine model of oleic acid-induced lung injury.

Perfluoroalkanes are also widely used in the chemical industry. For example, the linear perfluoroalkyl unit is present in most ZONYL intermediate surfactants as a mixture of chain lengths.[3] The distribution of these chains has concentrations up to 50% in n-C_6F_{14} and n-C_8F_{18} and up to 30% in n-$C_{10}F_{22}$, with average distributions of 7, 8, and 9 carbons. Moreover, short-chain perfluoroalkanes (n-C_6F_{14}−n-$C_{10}F_{22}$) can be added to colloids or nanoparticles to act as stabilizers in the presence of CO_2 and provide unique tools not only in process application but also in biomedical research.[4]

Carbon dioxide properties have been studied in academia and in industry in a continuous manner since the 1950s; however, in the past decade the studies have increased in an exponential fashion. This is principally due to the widely extended use of CO_2 in commercial plants as well as its potential use as a sustainable fluid for the protection of the environment, at least when compared to many common organic solvents. Several independent studies[5−8] have explored the utility of CO_2 over the last two decades, in which it has been used as a solvent, cosolvent, plasticizer, penetrant, and foaming agent.

It is, then, surprising that very little data (experimental or theoretical) is available in the open literature for these systems, limiting their use for present and future applications to a great extent. It is the objective of the present work to present, for the first time, phase equilibria diagrams for ternary, and in several cases binary, mixtures of CO_2/n-perfluoroalkanes/n-alkanes. We use the statistical associating fluid theory of variable range (SAFT-VR) for this purpose. We study the influence that temperature, pressure, composition, and chain length have on the phase diagram, showing that the predicted diagrams should represent the expected phase-equilibria behavior with good accuracy.

Model Description

The statistical associating fluid theory[9,10] (SAFT) is based on a resummed perturbation series due to Wertheim[11,12] and accounts in a realistic way for the association between molecules, in addition to dispersion plus repulsive interactions. Moreover, SAFT can account for chain effects including polymer molecules.

The SAFT equations have proved to be a significant improvement over the more empirical equations of state (EOS) because they have a firm basis in statistical mechanics. In SAFT,[9,10] molecules are modeled as chains of covalently bonded spheres. Homologous series, such as n-alkanes, n-perfluoroalkanes, and polymers, can be modeled as chains of identical spheres in which the number of spheres in the chain is proportional to the molecular weight. In SAFT, the residual Helmholtz energy, A^{res}, is of the form

$$\frac{A^{res}}{NkT} = \frac{A^{seg}}{NkT} + \frac{A^{chain}}{NkT} + \frac{A^{assoc}}{NkT} \quad (1)$$

* Corresponding author. E-mail: keg@ncsu.edu. Phone: +1 (911) 513 2262. Fax: +1 (919) 513 2470.

10.1021/jp046612d CCC: $30.25
Published on Web 01/29/2005

where A^{seg} is the part of the Helmholtz energy due to segment−segment interactions (interactions between monomer units, usually modeled as hard sphere, Lennard-Jones (LJ), or square-well interactions), A^{chain} is the additional Helmholtz energy due to chain formation, and A^{assoc} is that due to association (e.g., hydrogen bonding between different molecules). N is the number of molecules, k is the Boltzmann constant, and T is the temperature.

The most widely used version of SAFT is the implementation of Huang and Radosz[13] (SAFT-HR), who fitted the potential parameters to the experimental vapor pressure and saturated liquid-density data for more than 100 real fluids. For the segment term, they used the sum of a hard-sphere part given by the Carnahan−Starling equation[14] and a dispersion part given by the BACK equation of Chen and Kreglewski.[15] Some recent papers[16−19] compare the SAFT EOS and extensions of it to other existing methods. In general, the SAFT, with its more rigorous foundation, is found to be more reliable for both fitting data and prediction; in particular, this is the case for associating fluids and chain molecules.

Among several modifications, we would like to highlight the so-called Soft-SAFT, PC-SAFT, and SAFT-VR. The Soft-SAFT EOS[20,21] is a modification of the original SAFT equation proposed by Chapman et al.[10] in which the reference term is a Lennard-Jones fluid. Chapman[22] was the first to extend the equation to a reference fluid of Lennard-Jones spheres. In the Soft-SAFT version, the equation of Johnson et al.[23] is used for modeling the Lennard-Jones fluid. As in the rest of the SAFT equations, the chain contribution is obtained by Wertheim's first-order perturbation theory.[11,12] Blas and Vega have shown[20,21] that this version is very accurate in predicting the thermodynamic properties and phase equilibria behavior of model and real hydrocarbon mixtures. Recently, Dias et al.[24] studied binary mixtures of xenon or oxygen in *n*-perfluoroalkanes (n-C_1F_4 to n-C_8F_{18}) using this approach.

The model development of the PC-SAFT (perturbed-chain SAFT) equation of state is described in detail by Gross and Sadowski.[25] In contrast to the SAFT equation of state, the PC-SAFT model accounts for the nonspherical shape of the molecules also in the dispersion term. The perturbation theory of Barker and Henderson[26] was applied using a hard-chain fluid as the reference system, whereas a hard-sphere reference was considered in earlier SAFT models. The theory was tested for square-well chains versus computer simulations,[27] leading to a satisfactory prediction of the simulated behavior. Readjusting of the model constants for real substances led to the PC-SAFT EOS.[25]

Gil-Villegas et al.[28,29] proposed a version of SAFT with an attractive potential of variable range (SAFT-VR). In the framework of the perturbation theory, they deduced analytical perturbation expressions for the contribution of the Helmholtz free energy for several potentials, such as square-well, Sutherland, Yukawa, and Mie $m-n$ potentials. The incorporation of an additional nonconformal range parameter allows for an accurate description of the bulk thermodynamics of systems ranging from small strongly associating or polar molecules, such as water[30] and replacement refrigerants,[31] to long-chain alkanes[32] and polyethylene.[33] Moreover, linear perfluoroalkanes have been studied within the SAFT-VR approach by McCabe et al.[34] and Colina et al.[35] with the so-called SAFT-VR EOS. Galindo and Blas[36,37] studied the global phase behavior of carbon dioxide/*n*-alkane binary mixtures and compared the predictions of the SAFT-VR EOS with the extensive experimental data that is available for these mixtures. Recently,[35] we studied the phase behavior of binary mixtures containing carbon dioxide, *n*-alkanes (n-C_6H_{14}, n-C_7H_{16}, and n-C_8H_{18}), and *n*-perfluoroalkanes (n-C_6F_{14}, n-C_7F_{16}) with the same theory, and we found that it was in very good agreement with the available experimental data. These previous works provide a solid base from which to proceed, and we elected, then, to use the SAFT-VR EOS in this work for the prediction of ternary phase diagrams among carbon dioxide, *n*-perfluoroalkanes, and *n*-alkanes.

In the SAFT-VR approach,[28,29] the molecules are modeled as chains of tangentially bonded hard-spherical segments of diameter σ. The attractive interactions are described by a square-well potential of variable range (λ_{ij}) and depth (ϵ_{ij}), and the contribution to the free energy due to the dispersion interactions is obtained by following the framework of perturbation theory. Association interactions can also be considered through the embedded short-range attractive interaction sites. In this work, we treat nonassociating molecules, so this contribution is not necessary. The Helmholtz free energy (A) of an n-component mixture of CO_2, *n*-perfluoroalkane, and *n*-alkane molecules can be written as

$$\frac{A}{NkT} = \frac{A^{IDEAL}}{NkT} + \frac{A^{MONO}}{NkT} + \frac{A^{CHAIN}}{NkT} \tag{2}$$

The ideal contribution to the free energy is given by a sum over all species i in the mixture[28]

$$\frac{A^{IDEAL}}{NkT} = \sum_{i=1}^{n} x_i \ln(\rho_i \Lambda_i^{\,3}) - 1 \tag{3}$$

where $x_i = N_i/N$ is the mole fraction, $\rho_i = N_i/V$ is the number density, N_i is the number of molecules, V is the volume of the system, and Λ_i is the thermal de Broglie wavelength of species i. The monomer Helmholtz free energy can be written as[28−36]

$$\frac{A^{MONO}}{NkT} = \left(\sum_{i=1} x_i m_i\right)\left(a^{HS} + \frac{1}{kT}a_1 + \left(\frac{1}{kT}\right)^2 a_2\right) \tag{4}$$

where

$$a^{HS} = \frac{6}{\pi\rho_s}\left[\left(\frac{\zeta_2^{\,3}}{\zeta_3^{\,2}} - \zeta_0\right)\ln(1-\zeta_3) + \frac{3\zeta_1\zeta_2}{(1-\zeta_3)} + \frac{\zeta_2^{\,3}}{\zeta_3(1-\zeta_3)^2}\right] \tag{5}$$

$$a_1 = \sum_{i=1}^{n}\sum_{j=1}^{n} x_{s,i}x_{s,j}\left(-\frac{2}{3}\pi\epsilon_{ij}\sigma_{ij}^{\,3}(\lambda_{ij}^{\,3}-1)\rho_s g_0^{HS}(\sigma_\chi;\zeta_\chi^{eff})\right) \tag{6}$$

$$a_2 = \sum_{i=1}^{n}\sum_{j=1}^{n} x_{s,i}x_{s,j}\frac{1}{2}\epsilon_{ij}K^{HS}\rho_s\frac{\partial a_1^{\,ij}}{\partial\rho_s} \tag{7}$$

where m_i is the number of spherical segments of chain i, $\rho_s = N_s/V$ is the total number density of spherical segments, and ζ_i are the reduced densities. The mean attractive energy (a_1) is obtained from the sum of the partial terms corresponding to each type of pair interaction; $g_0^{HS}(\sigma_\chi;\zeta_\chi^{eff})$ is the contact radial distribution function of a hypothetical pure fluid of average diameter σ_χ. The effective packing fraction ζ_χ^{eff} is obtained from the corresponding packing fraction of the fluid ζ_χ, using $\zeta_\chi^{eff}(\zeta_\chi, \lambda_{ij}) = c_1(\lambda_{ij})\zeta_\chi + c_2(\lambda_{ij})\zeta_\chi^{\,2} + c_3(\lambda_{ij})\zeta_\chi^{\,3}$, where c_1, c_2, and c_3 are coefficients given in ref 28. Finally, K^{HS} is the hard-sphere isothermal compressibility of Percus−Yevick theory.[38]

TABLE 1: Optimized SAFT-VR Square-Well Intermolecular Potential Parameters

	m	λ	σ_c/Å[a]	ϵ_c/k (K)[a]
CO_2	2.0	1.5157	3.1364	168.89
C_6H_{14}	2.667	1.552	4.479	236.6
C_7H_{16}	3.0	1.563	4.529	237.3
C_8H_{18}	3.333	1.574	4.564	236.5
C_9H_{20}	3.667	1.602	4.545	227.4
$C_{10}H_{22}$	4.0	1.621	4.561	220.4
C_6F_{14}	2.85	1.4390	5.0315	264.24
C_7F_{16}	3.22	1.4365	5.1233	272.63
C_8F_{18}	3.59	1.4554	5.0694	270.51

[a] The subscript c indicates that the parameters have been rescaled to the experimental critical point.

The contribution to the free energy due to chain formation is expressed in terms of the contact value of the monomer background correlation function as[28−36]

$$\frac{A^{\mathrm{CHAIN}}}{NkT} = -\sum_{i=1}^{n} x_i(m_i - 1)\ln y_{ii}^{\mathrm{MONO}}(\sigma_{ii}) \qquad (8)$$

where, for square-well chains, $y_{ii}^{\mathrm{MONO}}(\sigma_{ii}) = y_{ii}^{\mathrm{SW}}(\sigma_{ii})$ and $y_{ii}^{\mathrm{SW}}(\sigma_{ii}) = g_{ii}^{\mathrm{SW}}(\sigma_{ii})\exp(\epsilon_{ii}/kT)$. In the SAFT-VR approach, the radial distribution function of the system of unbonded monomers is obtained from a high-temperature expansion $g_{ii}^{\mathrm{SW}}(\sigma_{ii}) = g_{ii}^{\mathrm{HS}}(\sigma_{ii}) + (\epsilon_{ii}/kT)g_1(\sigma_{ii})$, where the reference term is evaluated using the expression of Boublík.[39] Once the free energy is known, standard thermodynamic relations can be used to determine the pressure and chemical potentials, and the phase equilibrium conditions (equality of temperature, pressure, and chemical potentials of each component in all phases) can be solved using a numerical algorithm.[40]

Pure-Component Parameters. The first step in the application of the SAFT-VR to multicomponent mixtures (and any EOS in general) is to determine the intermolecular pure-component parameters. As we mentioned before, for a nonassociating component, there are four component parameters. m_i is the number of spherical segments in a chain, and this is treated as an adjustable parameter. The diameter of hard-spherical segments tangentially bonded together is σ. The attractive interactions are described by a square-well potential of variable range (λ_{ij}) and depth (ϵ_{ij}).

Galindo and Blas[36,37] obtained carbon dioxide (CO_2) parameters by fitting to experimental vapor pressures and saturated densities. CO_2 is modeled as a nonassociating and nonspherical molecule in which the nonspherical (i.e., linear) nature of the molecule is treated in an explicit way by modeling the molecule with two tangentially bonded square-well segments. The attractive dispersion interactions and the quadrupole are treated in an effective way via a square-well potential of depth ϵ_{ii} and adjustable range λ_{ii}. The *n*-alkane molecules have also been studied in a number of previous works with the SAFT-VR approach.[28,32,36] The number of segments (m_i) forming the model chain can be obtained as a function of the number of carbon atoms (C) of the *n*-alkane molecule by using $m_i = (C - 1)/3 + 1$. Using this value for m_i, McCabe and Jackson[32] have carried out the optimization of the monomer intermolecular parameters for a large number of *n*-alkanes (from methane to *n*-hexatriacontane) using experimental vapor pressures and saturated liquid densities; these values are used in this work. The parameters of carbon dioxide and *n*-alkanes are presented in Table 1 for completeness. Following previous works,[34] we related the number of segments (m_i) forming a model *n*-perfluoroalkane chain to the number of carbons (C) of the *n*-perfluoroalkane molecule by using $m_i = (C - 1)*0.37 + 1$. Using these values for m_i, McCabe et al.[34] presented parameters for perfluoromethane to *n*-perfluorobutane. Recently, we presented[35] the parameters for *n*-perfluorohexane and *n*-perfluoroheptane. In the case of *n*-perfluorooctane, some experimental data[41] for experimental vapor pressures and saturated liquid densities is available in the literature. The optimized intermolecular parameters for the *n*-perfluoroalkane molecules used in this work are also presented in Table 1.

TABLE 2: SAFT-VR Square-Well Intermolecular Potential Parameters for the Binary Mixtures

system[a]	ξ_{ij}	γ_{ij}
CO_2/*n*-C_nH_{2n+2}	0.88	0.989
CO_2/*n*-C_nF_{2n+2}	0.88	0.989
C_6F_{14}/*n*-C_nH_{2n+2}	0.929	1
C_7F_{16}/*n*-C_nH_{2n+2}	0.932	1
C_8F_{18}/*n*-C_nH_{2n+2}	0.932	1

[a] n: 6−10.

Mixture Parameters. The extension to multicomponent mixtures is straightforward with the SAFT EOS because the reference terms can be extended to mixtures on the basis of rigorous statistical mechanics. In the case of the SAFT-VR approach for nonassociating chain molecules, the calculation of mixture phase behavior requires the determination of a number of unlike intermolecular parameters; these are σ_{ij}, ϵ_{ij}, and λ_{ij}. Traditionally, the modified Lorentz−Berthelot combining rules are used[42]

$$\sigma_{ij} = \frac{\sigma_{ii} + \sigma_{jj}}{2} \qquad \epsilon_{ij} = \xi_{ij}\sqrt{\epsilon_{ii}\epsilon_{jj}} \qquad \text{and } \lambda_{ij} = \gamma_{ij}\frac{\lambda_{ii}\sigma_{ii} + \lambda_{jj}\sigma_{jj}}{\sigma_{ii} + \sigma_{jj}} \qquad (9)$$

In the case of hard core potentials, σ_{ij} is given exactly by the expression shown in eq 9 but the parameters describing the unlike square-well energy (ϵ_{ij}) and range (λ_{ij}) are only approximate, so two adjustable parameters (ξ_{ij} and γ_{ij}) often need to be introduced to improve the agreement with the experimental-mixture phase behavior. The adjustable parameters used in this work are presented in Table 2.

Values of $\xi_{\mathrm{alkane-CO_2}} = 0.88$ and $\gamma_{\mathrm{alkane-CO_2}} = 0.989$ were determined by Galindo and Blas[36,37] to ensure that the mixture of CO_2/*n*-$C_{13}H_{28}$ exhibits type-IV phase behavior in the classification of Scott and van Konynenburg.[43] The set of parameters that was used is not temperature-dependent, so it can be used to describe the phase behavior of the mixture for the entire fluid range and can be transferred to other CO_2/*n*-alkane mixtures.[36] This transferability was confirmed in our previous work[35] for mixtures of CO_2/*n*-hexane and CO_2/*n*-heptane. Here we show that the same parameters provide a good description of the vapor−liquid and vapor−liquid−liquid equilibria in binary and ternary mixtures.

In the case of the mixtures of CO_2/*n*-perfluorohexane and CO_2/*n*-perfluoroheptane, we found[35] that the same unlike adjustable intermolecular parameters can be used (i.e., $\xi_{\mathrm{perfluoroalkane-CO_2}} = 0.88$ and $\gamma_{\mathrm{perfluoroalkane-CO_2}} = 0.989$). The similarity to the *n*-alkane parameters was explained on the basis of the use of square-well potentials to treat the quadrupolar interactions characteristic of carbon dioxide in an effective way, and parameters ξ_{ij} and γ_{ij} mainly provide a correction for this approximation. Moreover, this previous work supports the proposition that the increased solubility of *n*-perfluoroalkanes in CO_2 may be closely related to larger attractive dispersion

interactions. For a complete discussion of this topic, we refer the reader to our previous work.[35]

Binary *n*-alkane/*n*-perfluoroalkane mixtures are known to exhibit type-II phase behavior in the classification of Scott and van Konynenburg[43] when the difference in chain length between the two components is not very large ("symmetric" (same carbon number) or close-to-symmetric systems). Mixtures of the components considered in this work exhibit this type of phase diagram. McCabe et al.[33] studied the high-pressure phase behavior of a number of *n*-perfluroalkane (*n*-C_1F_4−*n*-C_4F_{10}) and *n*-alkane (*n*-C_1H_4−*n*-C_7H_{16}) systems and suggested a value of $\xi_{\text{alkane-perfluoroalkane}} = 0.9234$ (with $\gamma_{\text{alkane-perfluoroalkane}} = 1$, as could be expected because both molecules are nonpolar) for the symmetric case and $\xi_{\text{alkane-perfluoroalkane}} = 0.9206$ or 0.8948 for unsymmetrical cases. We found[35] that the slightly different value of $\xi_{\text{alkane-perfluoroalkane}} = 0.929$ (with $\gamma_{\text{alkane-perfluoroalkane}} = 1$) provides a better fit to the upper critical solution temperatures[44] (UCST) of *n*-C_6H_{14}/*n*-C_6F_{14} and *n*-C_7H_{16}/*n*-C_6F_{14}. In figure 5

of our previous work,[35] we erroneously labeled the *x* axis as well as the legend of this figure. The *x* axis should read X (C_6F_{14}), and the figure is for the liquid−liquid equilibrium of the *n*-hexane/*n*-perfluorohexane and *n*-heptane/*n*-perfluorohexane binary mixtures, as compared to the SAFT-VR predictions. In addition, the closed symbols represent the experimental data for $C_7H_{16} + C_6F_{14}$ of ref 56 of the cited work. This does not alter the results and/or conclusions presented in any way. The influence of the value of the $\xi_{\text{alkane-perfluoroalkane}}$ parameter on the equilibrium conditions will be discussed in the next section.

It is important to mention that all of the values for unlike parameters (binary interaction parameters) mentioned above are within the expected range for a binary interaction parameter (i.e., between 0.85 and 1.15 or −0.15 to 0.15, depending on the definition used). It is essential to keep in mind that binary interaction parameters are used to "correct" a theory in a way so that real systems can be represented with higher accuracy. Greater values of these parameters would indicate that the model (or combining rule) employed is not the most adequate to represent the system under investigation and modifications or different models should be utilized. We stress that the present rule of thumb is valid for interaction parameters in any model or combining or mixing rule.

In the next section, we show that the SAFT-VR EOS predicts the vapor−liquid equilibria (VLE), liquid−liquid equilibria (LLE), and vapor−liquid−liquid equilibria (VLLE) of binary and ternary mixtures of *n*-alkanes, *n*-perfluoralkanes, and CO_2 in very good agreement with the available experimental and molecular simulation data.

Results and Discussion

One-, two- and three-phase regions can exist simultaneously in ternary systems at particular temperatures and pressures, yet only one or two of each one- or two-phase region are present in the majority of the systems that have been investigated to date.[45] The shapes of such regions may differ markedly from system to system or with the range of conditions. The reader is referred to Wallas' book[45] for an introductory but comprehensive discussion of ternary phase diagrams.

Fifty years ago, Francis[46] presented a set of 464 qualitative ternary diagrams with (liquid) carbon dioxide as one of the components, displaying a great variety of behavior at or near room temperature and around 6.6 MPa. Even though the triangular graphs presented were qualitative, they represented

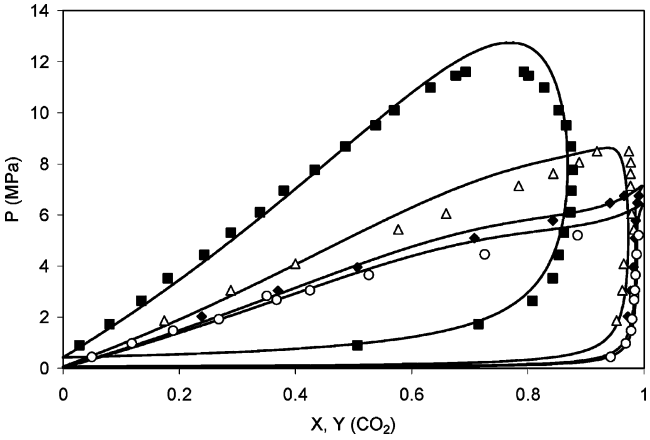

Figure 1. Vapor−liquid equilibrium of the CO_2/*n*-hexane binary mixture compared to that of the SAFT-VR predictions. Symbols represent the experimental data at (○) 298,[48] (◆) 303,[49] (△) 323,[49] and (■) 393 K.[50] The theoretical predictions are shown by the continuous curves.

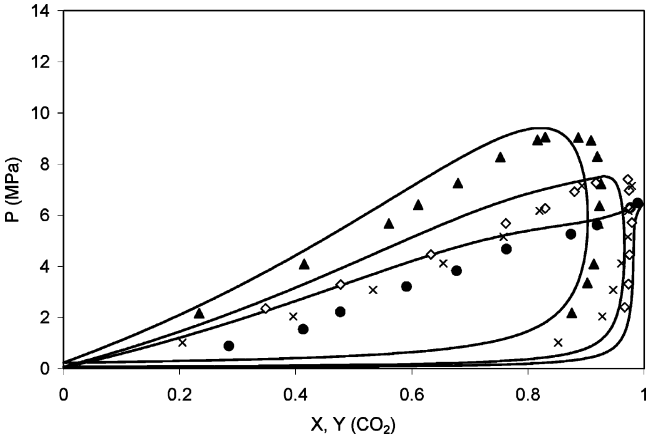

Figure 2. Vapor−liquid equilibrium of the CO_2/*n*-perfluorohexane binary mixture compared to that of the SAFT-VR predictions. Symbols represent the experimental data at (●) 298,[51] (◇) 314.65,[52] and (▲) 353 K;[48] crosses correspond to the molecular simulations of Zhang and Siepmann[58] at 315 K. The theoretical predictions are shown by the continuous curves.

a vast amount of information for the 261 substances studied. Unfortunately, perfluoroalkanes were not included in that study and neither was the effect of temperature or pressure. An example of the influence of pressure and temperature on three-phase behavior (LLLE) is given in the work of Andersen et al.[47] for mixtures of water/*n*-alkyl polyoxyethylene ether/*n*-alkane systems.

CO_2/*n*-Perfluorohexane/*n*-Alkane Phase Equilibria. In a recent work,[35] we found excellent agreement for the vapor−liquid equilibria (VLE) of the CO_2/*n*-C_6H_{14} mixture when comparing it to the available experimental data at 313 and 353 K. Additionally, we found very good predictions for the VLE of CO_2/*n*-C_6F_{14} at the same temperatures and for VLE and liquid−liquid equilibria (LLE) of *n*-C_6H_{14}/*n*-C_6F_{14}. In this section, we present the ternary diagrams that were obtained for the CO_2/*n*-C_6F_{14}/*n*-C_6H_{14} mixture as a function of temperature and pressure. For the sake of completeness, we also present some binary diagrams.

In Figure 1, the VLE predictions of the CO_2/*n*-C_6H_{14} mixture at different temperatures (298, 303, 323, and 393 K) are compared to the available experimental data.[48−50] In general, good agreement is found. In this Figure, it can be seen that the theory predicts coexisting liquid compositions that are somewhat

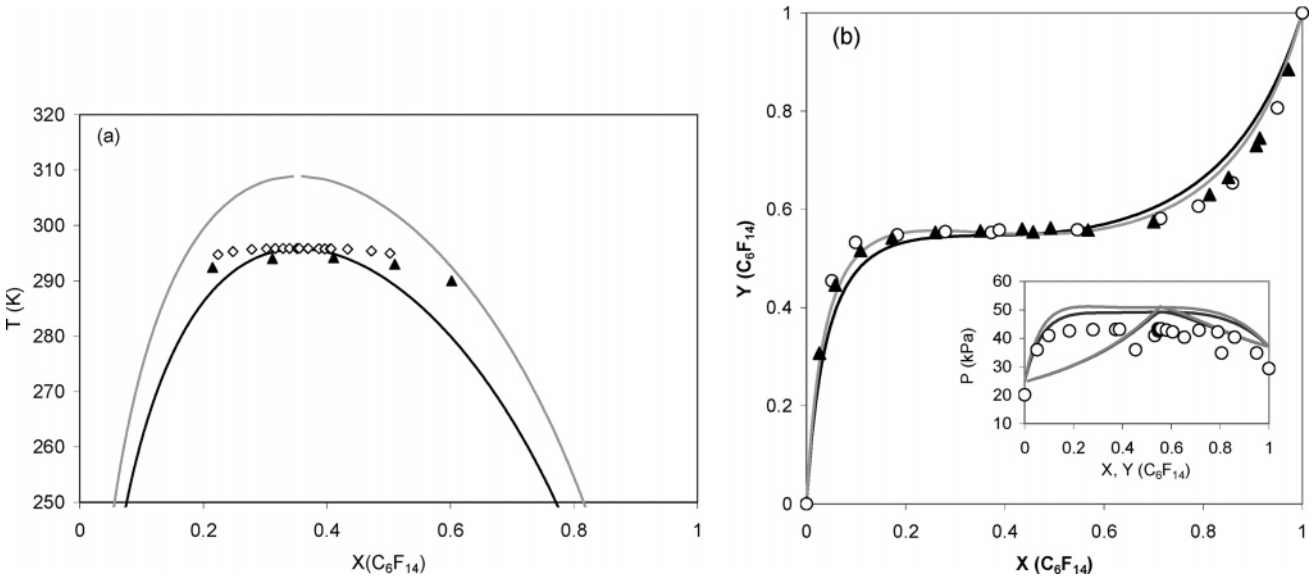

Figure 3. (a) Liquid−liquid and (b) vapor−liquid equilibrium of the *n*-hexane/*n*-perfluorohexane binary mixture compared to that of the SAFT-VR predictions for two different unlike parameters. Symbols represent the experimental data of (▲) Duce et al.,[53] (◇) Gaw et al.,[54] and (○) Dunlap et al.[55] The theoretical predictions are shown by the continuous lines. The bold line corresponds to $\xi = 0.929$, and the gray line corresponds to $\xi = 0.9234$.

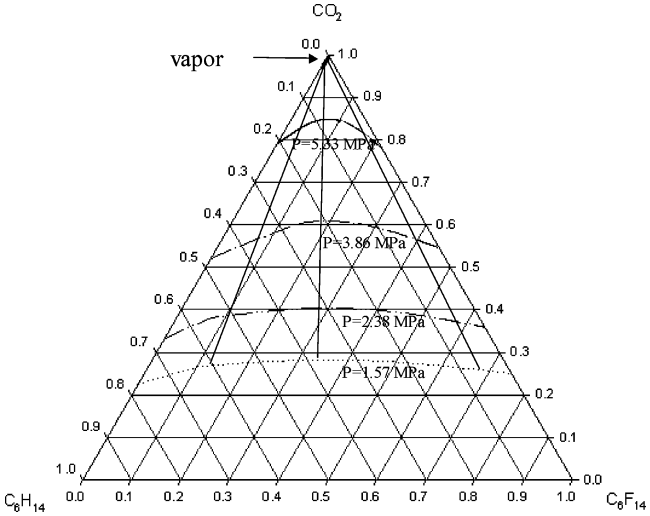

Figure 4. SAFT-VR predictions for the vapor−liquid equilibrium (VLE) of the CO_2/*n*-perfluorohexane/*n*-hexane system at 298.15 K. Dotted line, 1.57 MPa; double-dotted dashed line, 2.38 MPa; dotted dashed line, 3.86 MPa; continuous line, 5.33 MPa.

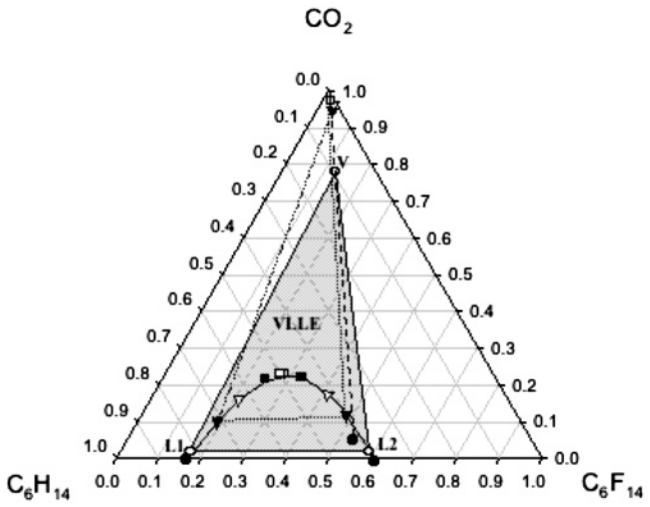

Figure 5. SAFT-VR predictions for the vapor−liquid−liquid equilibrium (VLLE) of the CO_2/*n*-perfluorohexane/*n*-hexane system at 278.15 K. Liquid−liquid equilibria, continuous bold line; vapor phase in equilibrium with liquid−liquid phases, dashed line. Symbols correspond to the points in the equilibrium at constant pressure: (●) 22.75, (○) 101.05, (▼) 471.88, (▽) 783.16, (■) 943.24, and (□) 986.14 kPa.

too small at low temperatures and pressures that are too high at the highest temperature studied. Similarly, in Figure 2 we present the VLE predictions of CO_2/*n*-C_6F_{14} at different temperatures (298, 314.65, and 353 K) and compare them to the available experimental[49,51,52] and molecular simulation[58] data. An underprediction is found for the liquid compositions at 298 K; this is less pronounced at the other temperatures. However, it is important to keep in mind that these calculations are totally predictive (i.e., they were obtained from pure-component parameters and a set of binary interaction parameters that are neither fluid- nor temperature-dependent).[35−37]

In Figure 3a, the LLE of *n*-C_6F_{14}/*n*-C_6H_{14} is presented for two different unlike intermolecular parameters and compared to the available experimental data. The bold line represents the predictions obtained from a fit ($\xi = 0.929$) of the UCST of the *n*-C_6F_{14}/*n*-C_6H_{14} system in our previous work.[35] The gray line corresponds to the value for symmetric systems suggested by Mc Cabe et al.[34] ($\xi = 0.9234$; this value was obtained from a fit of the UCST of the *n*-C_4F_{10}/*n*-C_4H_{10} mixture) and used here as a transferable parameter. The predictions with both parameters are shown in this Figure to demonstrate the high impact that the selection of this parameter has on the LLE. However, the VLE do *not* strongly depend on the value of this parameter, as can be seen in Figure 3b. It is well known that choosing parameters to provide the best agreement with the critical point (UCST) of a mixture is to the detriment of the prediction of the compositions of the liquid phases.[35] Because the SAFT-VR is a classical, mean-field equation of state, in common with nearly all equations of state, it predicts a parabolic curve instead of the experimentally found cubic curve in the critical region; the latter arises from the nonanalytic nature of the coexistence in the critical region, which yields a much flatter curve in this region.

The UCST of *n*-C_6F_{14}/*n*-C_6H_{14} mixtures has been reported[56] to be 295.9 K. At temperatures greater than this value and in the presence of CO_2, only two phases (vapor−liquid) are present.

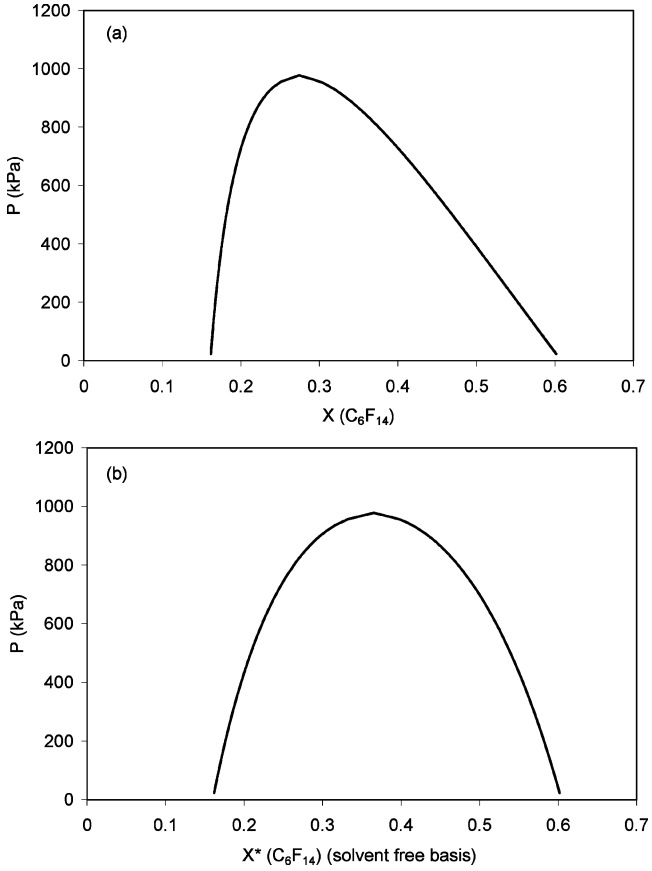

Figure 6. SAFT-VR predictions for the vapor−liquid−liquid equilibrium (VLLE) of the CO_2/*n*-perfluorohexane/*n*-hexane system at 278.15 K. Pressure (a) as a function of the composition of *n*-perfluorohexane in the liquid phases and (b) as a function of *n*-perfluorohexane in the liquid phases on a CO_2-free basis. The theoretical predictions, with $\xi = 0.929$, are shown by the continuous line. The pressure−composition diagrams show the pressure along the liquid−liquid coexistence curve.

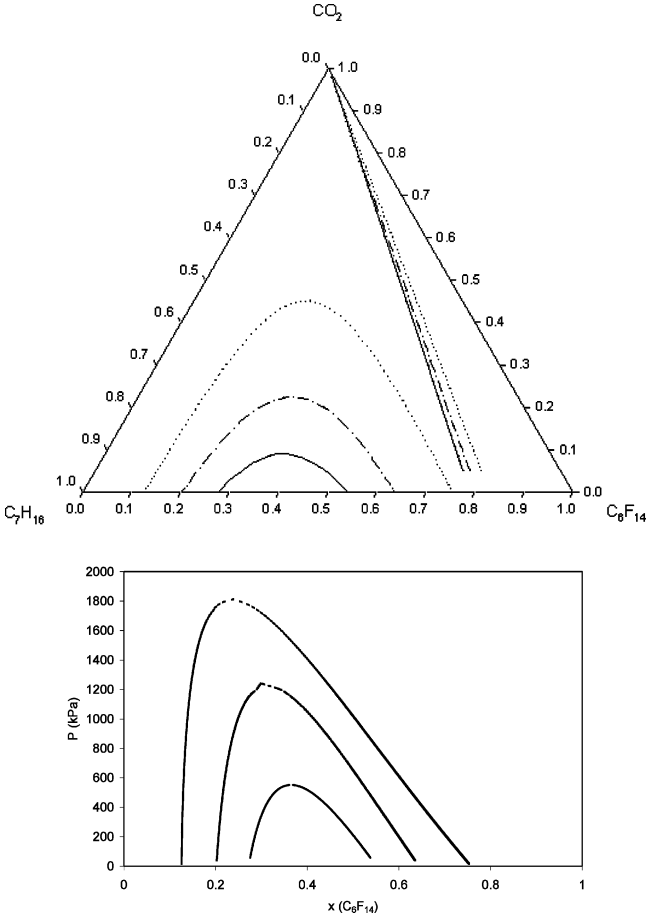

Figure 7. SAFT-VR predictions for the vapor−liquid−liquid equilibrium (VLLE) of the CO_2/*n*-heptane/*n*-perfluorohexane system at 278.15 (dotted line), 298.15 (dotted-dashed line), and 308.15 K (continuous line).

In Figure 4, we present the vapor−liquid equilibria (VLE) of the CO_2/*n*-C_6F_{14}/*n*-C_6H_{14} system at 298.15 K. Different isobars are presented. Vapor compositions are in the upper corner of the Figure, in the region shown by the arrow, and liquid compositions lie along the isobars shown. Only a few tie lines, at 1.57 MPa, are shown for clarity. We note that the intersection of these tie lines with the other isobars has no physical meaning. Pressure increases from 1.57 to 5.33 MPa, and as the pressure increases, the liquid-phase region increases, as should be expected.

The vapor−liquid−liquid equilibrium (VLLE) of the CO_2/*n*-C_6F_{14}/*n*-C_6H_{14} system at 278.15 K is presented in Figure 5. In this Figure, the continuous line represents the liquid phases in equilibrium with the vapor phase (represented by the dashed line). Selected points in equilibrium are shown with different symbols, and two VLL equilibrium states are highlighted. For example, the VLLE at 101.05 kPa and 278.15 K is indicated by the open circles, and the tie lines among them, by the lines that form the gray triangle. Any set of compositions (or global composition) that is inside of this triangle at the temperature and pressure given above will be a metastable condition, and the system will phase separate to form three phases in equilibrium (V, L1, and L2, represented by the open circles). At a different pressure (e.g., 471.88 kPa) and the same temperature, the three phases in equilbrium are represented by the filled triangles. Tie lines, in this case, are shown by the dotted lines connecting the filled triangles, and again at these temperature and pressure conditions (278.15 K, 471.88 kPa) any set of compositions inside the triangle formed by the dotted lines will phase separate to the equilibrium conditions shown by the filled triangles. At the baseline describing the *n*-perfluoroalkane/*n*-alkane binary mixture, the composition of carbon dioxide goes to zero, and thus the gas phase disappears. Note that the solid circles at the bottom of the diagram do not lie exactly on the two-phase line (i.e., they correspond to a ternary system). In our previous work,[35] we found that the LLE of the binary system *n*-C_6F_{14}/*n*-C_6H_{14} at 278.15 K is at $X^{I}(C_6F_{14}) = 0.1572$ and $X^{II}(C_6F_{14}) = 0.6124$. These are consistent with the results presented in this Figure (also see Table A1 of the Supporting Information). The equilibrium pressure changes over the set of conditions in this graph: the pressure increases as the amount of CO_2 in the liquid phases increases (i.e., the immiscibility gap among the *n*-perfluoroalkane-rich liquid phase and the *n*-alkane-rich liquid phase decreases with increasing pressure (and carbon dioxide content) at a constant temperature).

For clarity, the pressure as a function of *n*-perfluorohexane composition in the liquid phases is shown in Figure 6a (and in Figure 6b as a function of *n*-perfluorohexane composition in the same phases but on a CO_2-free basis (without CO_2)). As an example, we select the 101.05 kPa isobar (open circles). The *n*-perfluorohexane compositions can be read from the base axis (from left to right) of the ternary diagram. The *n*-perfluorohexane composition is ∼0.16 for the L1 phase and ∼0.6 for the L2 phase. From Figure 6a, it can be seen that at ∼100 kPa the *n*-perfluorohexane compositions of the two liquid phases in equilibrium are ∼0.16 and 0.59. Thus, the Figures presented

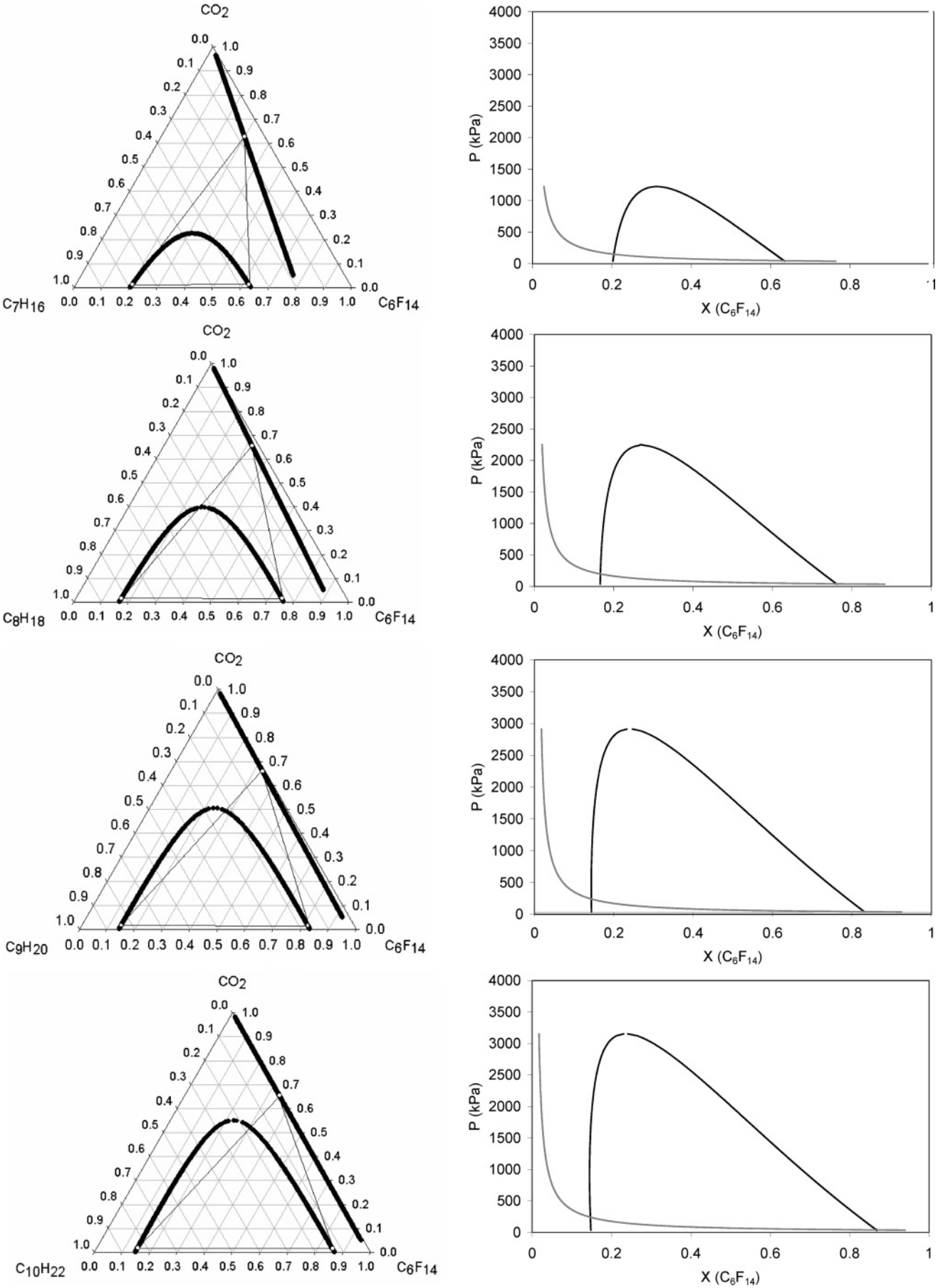

Figure 8. SAFT-VR predictions for the vapor−liquid−liquid equilibrium (VLLE) of the CO_2/*n*-perfluorohexane/C_nH_{2n+2} system at 298.15 K for $n = 7-10$. The pressure−composition diagrams show (a) the pressure along the liquid−liquid coexistence curve as a black line and (b) the pressure along the vapor phase curve as a gray line.

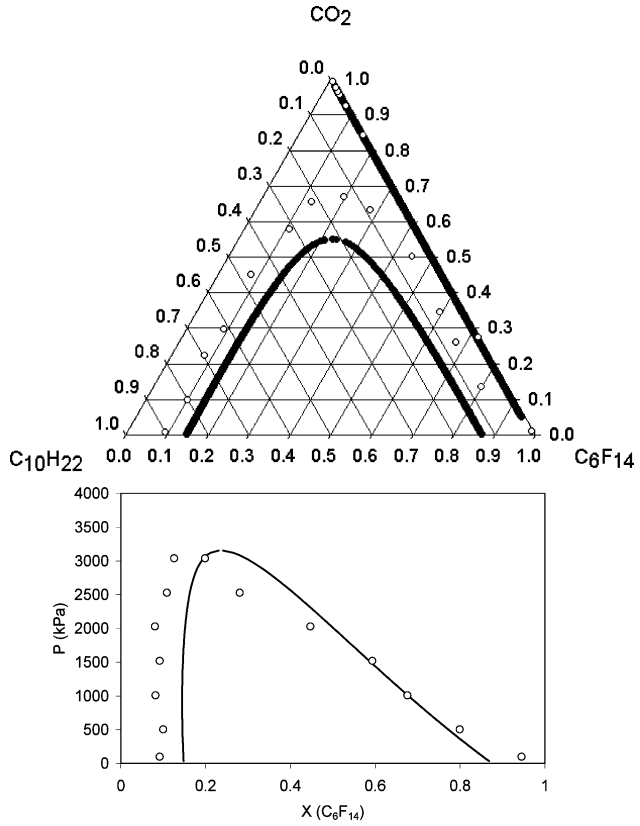

Figure 9. SAFT-VR predictions for the vapor−liquid−liquid equilibrium (VLLE) of the CO_2/*n*-perfluorohexane/*n*-decane system at 298 K. Symbols correspond to the molecular simulations of Zhang and Siepmann.[58] The theoretical predictions of this work are shown by the continuous lines.

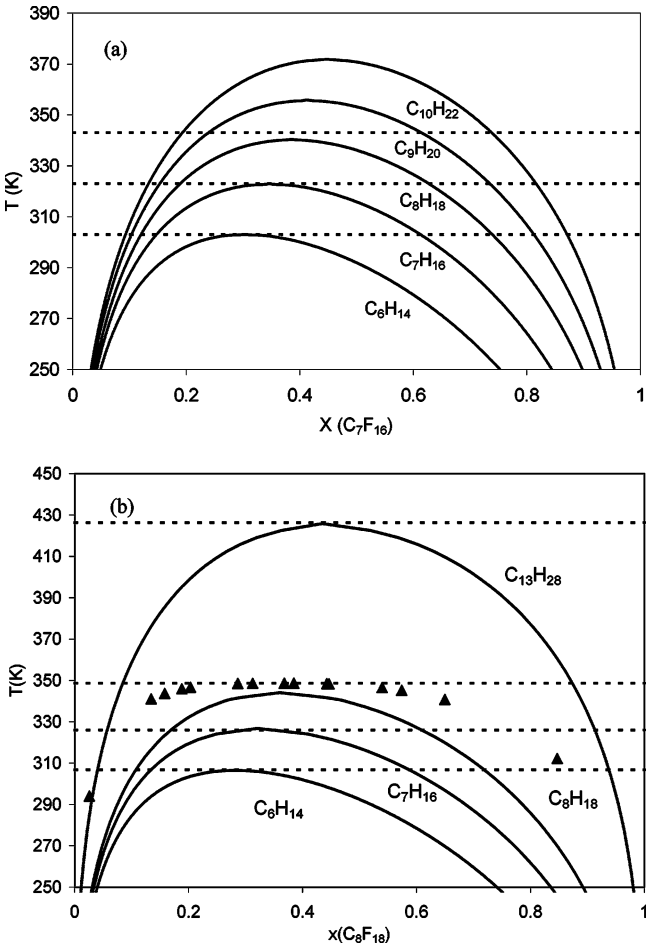

Figure 10. Liquid−liquid equilibrium of the (a) *n*-perfluoroheptane/*n*−C_nH_{2n+2} and (b) *n*-perfluorooctane/*n*-C_nH_{2n+2} binary mixtures compared to those of the SAFT-VR predictions for $n = 7-13$. Symbols represent the experimental data of (▲) Duce et al.,[53] and dotted lines represent the upper critical solution temperature reported by Christou et al.[59] The theoretical predictions, obtained with $\xi = 0.932$ in all cases, are shown by the continuous lines.

in this work can help us understand the thermodynamic behavior of the ternary systems studied here. However, these Figures cannot reproduce the accuracy of the predicted results. We have therefore presented some selected *PTx* equilibria points in several tables (A1 to A4) as Supporting Information that will allow the reader to have a good estimation for the selected system. In the case of Figure 5 for the CO_2/*n*-C_6F_{14}/*n*-C_6H_{14} system at 278.15 K, the results can be found in Table A1 (Supporting Information). It is important to notice that the CO_2 compositions were not explicitly tabulated because they can be easily obtained from the sum condition ($X(CO_2) = 1 - X(C_6F_{14}) - X(C_nH_{2n+2})$). CO_2-free compositions (X*) for Figure 6b can be easily calculated from $X(C_6F_{14})^* = X(C_6F_{14})/(1 - X(C_nH_{2n+2}))$.

It can be seen from these Figures that *n*-C_6F_{14} and *n*-C_6H_{14} become completely miscible at approximately 986 kPa in the presence of carbon dioxide. It is important to note, however, that as a consequence of the adjustment of the $\xi_{\text{alkane-perfluoroalkane}}$ parameter to the UCST of the *n*-alkane/*n*-perfluoroalkane system very good pressure predictions are obtained but the compositions of the two liquid phases in coexistence should be underpredicted (see Figure 3). (In other words, the predicted liquid−liquid immiscibility gap is somewhat narrower than the one that would be obtained if experiments (or molecular simulations) were performed, as will become evident for the CO_2/*n*-C_6F_{14}/*n*-$C_{10}H_{22}$ system, for which molecular simulation data is available.)

The influence of temperature on CO_2/*n*-perfluoralkane/*n*-alkane mixtures is shown in Figure 7 with CO_2/*n*-C_6F_{14}/*n*-C_7H_{16} as an example. It can be seen that the liquid−liquid immiscibility region decreases with increasing temperature, as expected. However, the influence of temperature on the vapor phase is less marked. It is also important to keep in mind that in the ternary plots presented in this work the pressure of the system increases as the amount of CO_2 increases.

In Figure 8, ternary diagrams are shown for the CO_2/*n*-C_6F_{14}/*n*-C_nH_{2n+2}, $n = 7-10$ systems at 298.15 K, in which LLVE is present in all of the systems at these conditions. The CO_2/*n*-C_6F_{14}/*n*-C_6H_{14} system is not included here because it does not present LLV equilibria at 298.15 K (see Figure 4). A single set of tie lines for an equilibrium condition (at 101.325 kPa) is shown. As expected, the theory predicts that the liquid−liquid immiscibility region increases with the carbon number of the *n*-alkane chain. It can also be observed that the partition of the *n*-alkane and *n*-perfluorohexane decreases in the vapor phase (whereas the *n*-alkane carbon number increases) until only almost-pure carbon dioxide is present. This plot can be very useful because it not only specifies the amount of material required to obtain the homogeneous (or heterogeneous, as desired) liquid phase but also indicates the partition coefficients of the components in different phases. This information could be used to guide experiments. In the CO_2/*n*-C_6F_{14}/*n*-C_7H_{16} system, it was found experimentally[57] that at room temperature the minimum pressure needed to obtain LVE was 1.5 MPa. This result agrees with our predictions shown in Figure 8, in which LLVE is predicted for pressures of 1.22 MPa or below. Moreover, Zhang and Siepmann[58] have recently reported LLVE

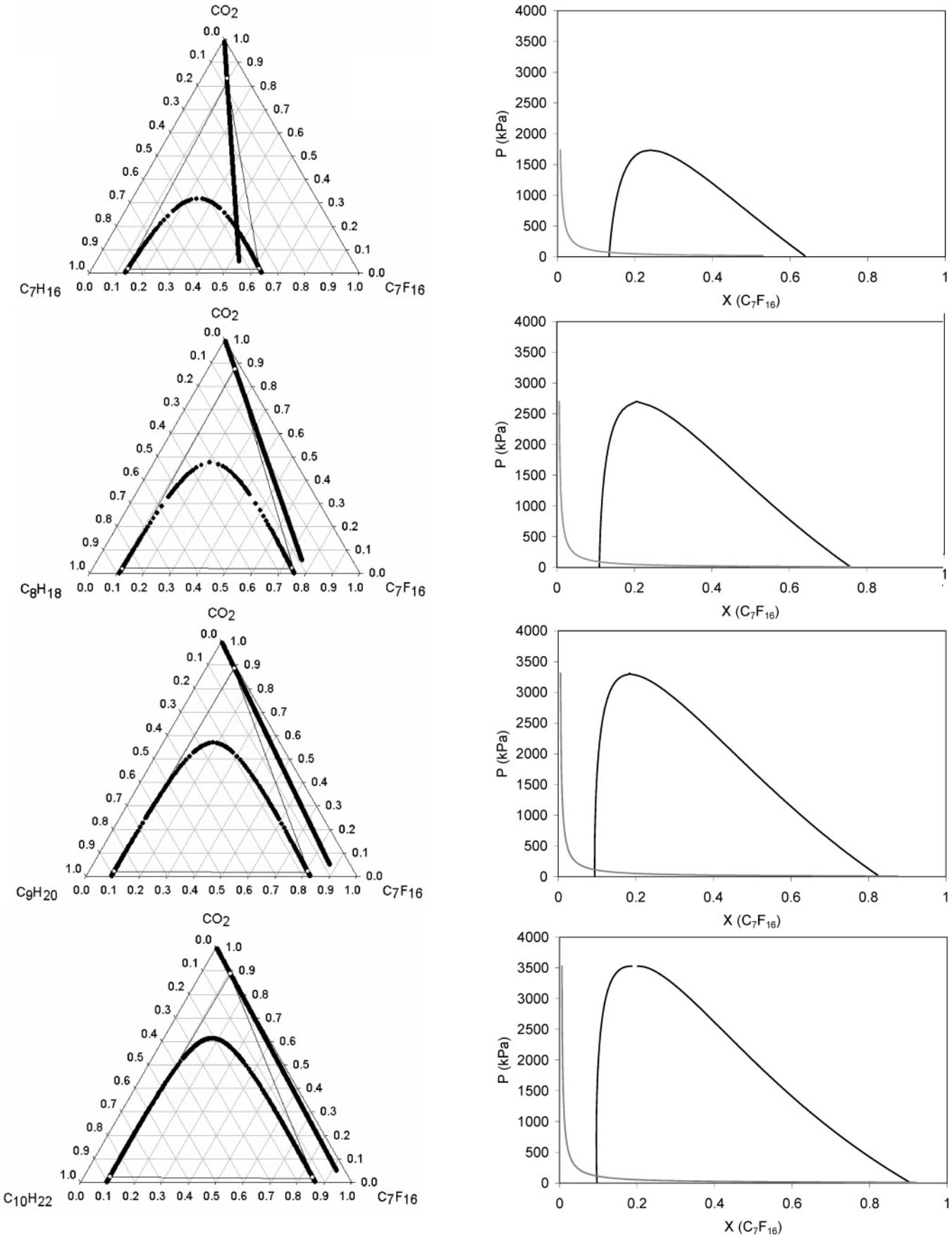

Figure 11. SAFT-VR predictions for the vapor−liquid−liquid equilibria (VLLE) of the CO_2/*n*-perfluoroheptane/*n*-C_nH_{2n+2} system at 298 K for $n = 7-10$.

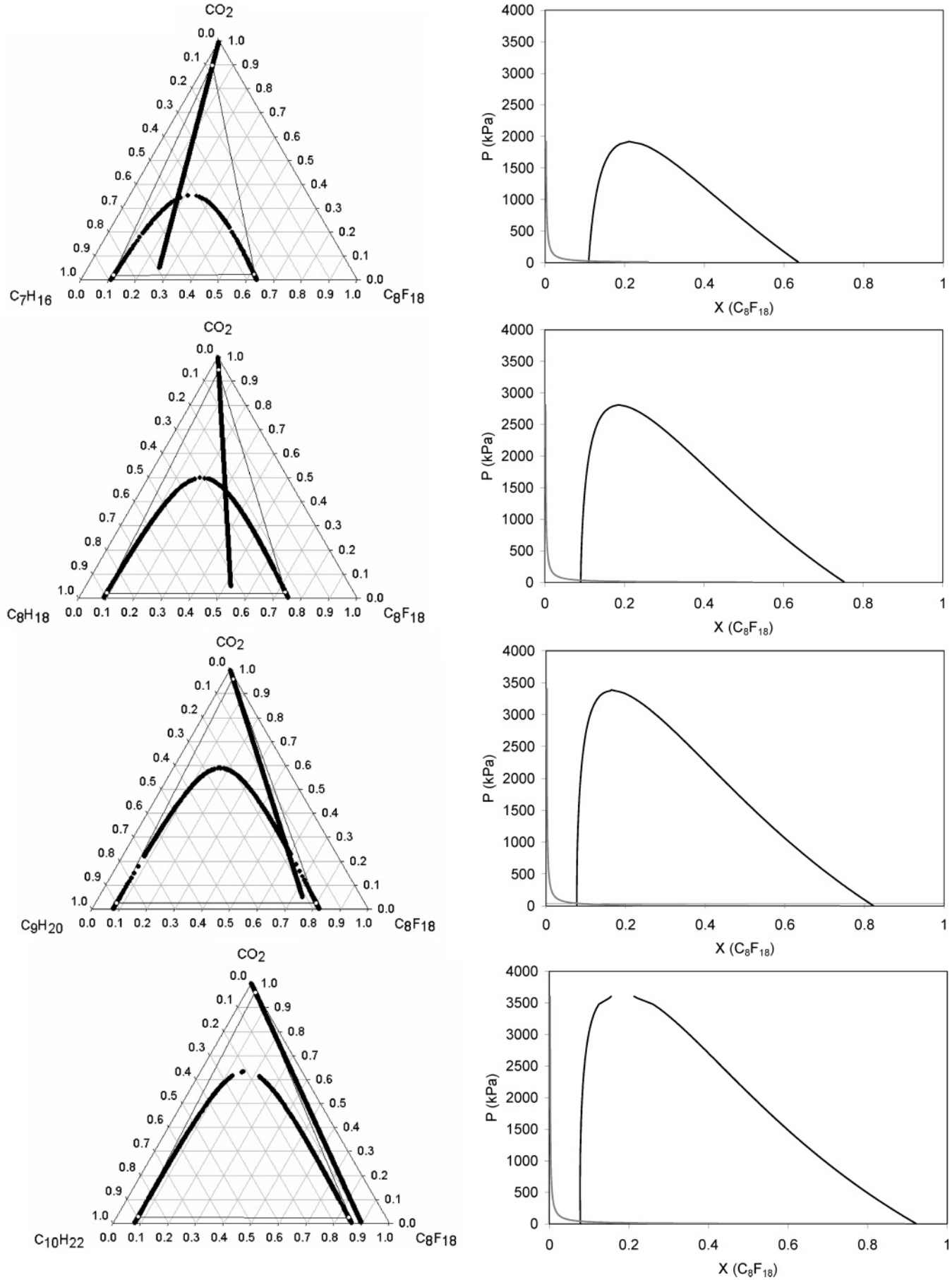

Figure 12. SAFT-VR predictions for the vapor−liquid−liquid equilibria (VLLE) of the CO_2/*n*-perfluorooctane/*n*-C_nH_{2n+2} system at 298 K for $n = 7-10$.

predictions obtained from Monte Carlo simulations of the CO_2/*n*-C_6F_{14}/*n*-$C_{10}H_{22}$ system at 298 K. The comparison between our results and their predictions are shown in Figure 9. The agreement between both methods is encouraging because very similar results were obtained from two independent studies. In this system, the SAFT-VR EOS predicts an upper critical miscibility pressure of 3.15 MPa, whereas Zhang and Siepmann predict a pressure of 3.3 MPa from Monte Carlo simulations. The good agreement in pressure (Figure 9b) from our predictions and the Monte Carlo simulations is gratifying; however, the compositions are underpredicted by the theory. Although molecular simulations can provide a deeper understanding because molecular structures can be observed, results from a molecular-based equation of state, such as the SAFT-VR, can provide rapid and accurate predictions and the calculations are at least 3 orders of magnitude faster. This feature permits systematic studies for different sets of conditions, as shown in this work. Moreover, these results can be used to guide experiments and at the same time provide insight into the underlying thermodynamics. In this respect, selected equilibrium points for the CO_2/*n*-C_6F_{14}/*n*-C_nH_{2n+2} ($n = 7-10$) systems are given in Table A2 (Supporting Information).

CO_2/*n*-Perfluoroheptane/*n*-Alkane or CO_2/*n*-Perfluorooctane/*n*-Alkane Phase Equilibria. For the rest of the triangular diagrams shown in this paper, we also elected to use a binary interaction parameter for the *n*-alkane/*n*-perfluoralkane interaction that provides a good prediction of the UCST of the liquid phases. This results in liquid−liquid subcritical compositions that are underpredicted. We found that this binary interaction parameter is dependent on the perfluoroalkane under study. For example, Figures 3−9 were generated with a constant value ($\xi_{\text{alkane-perfluorohexane}} = 0.929$). This unique value was obtained from a fit of the UCST of the *n*-C_6F_{14}/*n*-C_6H_{14} system and was used in a transferable fashion (giving excellent predictions, as shown in Figures 3−9) for all of the mixtures among *n*-perfluorohexane and the *n*-alkanes (C_6-C_{10}).

In Figure 10a, we show the LLE among *n*-perfluoroheptane and *n*-alkanes, and in Figure 10b, among *n*-perfluorooctane and *n*-alkanes, predicted with $\xi_{\text{alkane-perfluoroheptane}} = \xi_{\text{alkane-perfluorooctane}} = 0.932$ and adjusted to the UCST of *n*-C_8F_{18}/*n*-C_6H_{14}. Also shown (as dotted lines in the Figures) are the experimental UCST values. The agreement is excellent in general, especially taking into account that the binary interaction parameter, used here in a transferable fashion, was adjusted to only one UCST (that for *n*-C_8F_{18}/*n*-C_6H_{14} mixtures). Moreover, Figure 10b shows the prediction for the *n*-C_8F_{18}/*n*-$C_{13}H_{28}$ system, which is in excellent agreement with the experimental UCST for this system.

It is important to note, however, that different interaction parameters were obtained for $\xi_{\text{alkane-perfluorohexane}}$ and $\xi_{\text{alkane-perfluoroheptane.}}$ This is in contrast to our previous work.[35] In our previous work, we reported a unique binary interaction parameter of 0.929 for both *n*-perfluoroalkanes. However, in the previous work,[35] we evaluated only *n*-perfluoroheptane/*n*-alkane systems for VLE. As was shown in Figure 3, this parameter has practically no influence on the VLE but a strong influence on the LLE and, therefore, the LLVE for ternary systems. It appears that to provide good predictions for the LLE and VLLE for both binary and ternary systems the predicted UCST for each *n*-perfluoroalkane with a given *n*-alkane (in the range studied in this work) should be adjusted. Thus, only one experimental mixture point (the UCST of a binary *n*-alkane/*n*-perfluoroalkane mixture) is needed to adjust the binary interaction parameter for each *n*-perfluoroalkane, and then it can be used in a transferable fashion. The binary interaction parameters used in this work are shown in Table 2.

In Figures 11 and 12, ternary diagrams are shown for the CO_2/*n*-C_7F_{16}/*n*-C_nH_{2n+2} and CO_2/*n*-C_8F_{18}/*n*-C_nH_{2n+2} systems, with $n = 7-10$ at 298.15 K. Selected equilibrium points are presented in Tables A3 and A4 (Supporting Information) for the same systems. LLVE is present in all of the systems at these conditions. Similar to Figure 8, the theory predicts, as expected, that the liquid−liquid immiscibility region increases as the carbon number of the *n*-alkane chain increases. It can also be observed that the partition of the *n*-alkanes and *n*-perfluoroheptane or *n*-perfluorooctane decreases in the vapor phase as the *n*-alkane carbon number increases, until the vapor is almost pure carbon dioxide. Comparing Figures 8, 11, and 12, it is clear that at a constant temperature (298.15 K) and with a constant *n*-alkane (e.g., *n*-C_7H_{16}) the vapor composition shifts to the alkane-rich side of the triangular diagram as the molecular weight of the *n*-perfluoroalkane increases. This is due to the fact that the *n*-perfluoroalkane chain is longer and, then, less soluble in the vapor phase. Similarly, it can be observed that the pressure necessary to achieve miscibility of the liquid phases almost doubles from *n*-C_6F_{14} to *n*-C_8F_{18} (when the alkane is *n*-C_7H_{16}).

These ternary plots represent, to the best of our knowledge, the first available data for the *n*-perfluoroalkanes (*n*-C_6F_{14}, *n*-C_7F_{16}, *n*-C_8F_{18}), *n*-alkanes (*n*-C_6F_{14} to *n*-$C_{10}F_{22}$), and CO_2 systems. This information could be used to guide future experiments.

Conclusions

In this work, we presented vapor−liquid and vapor−liquid−liquid equilibria for ternary and several binary systems involving CO_2, *n*-alkanes, and *n*-perfluoroalkanes. We used, for this purpose, the SAFT-VR EOS and studied the influence of temperature, pressure, composition, and chain length on the phase diagram and showed that when compared to the available experimental and molecular simulation data the predicted phase diagrams should represent the expected phase equilibria behavior with good accuracy.

Our results show that it is possible to predict the overall phase behavior of different binary and ternary mixtures involving carbon dioxide, *n*-perfluoroalkanes, and *n*-alkanes using transferable binary interaction parameters. Upper critical solution pressures for several *n*-alkane/*n*-perfluoroalkane systems are also provided. Moreover, the ternary diagrams presented in this work represent, to the best of our knowledge, the first available data for CO_2/*n*-perfluoroalkane/*n*-alkane systems. The data provided in this work could be helpful in identifying possible new CO_2-philic groups as well as cosolvents for CO_2.

Acknowledgment. We thank Amparo Galindo, J. Ilja Siepmann, and Ling Zhang for helpful discussions. We also thank A.G. for providing the main routine of the SAFT-VR EOS. C.M.C. thanks Valery Bondar, Francisco Hung, Erik Santiso, and Claudio Olivera-Fuentes for helpful comments. This work was supported by the STC Program of the National Science Foundation under agreement no. CHE 9876674.

Supporting Information Available: *PTx* equilibria points of ternary systems. This material is available free of charge via the Internet at http://pubs.acs.org.

References and Notes

(1) Bleyl, J. U.; Ragaller, M.; Tscho, U.; Regner, M.; Hubler, M.; Kanzow, M.; Vincent O.; Albrecht, M. *Crit. Care Med.* **2002**, *30*, 1340.

(2) Riess, J. G. *Chem. Rev.* **2001**, *101*, 2797.
(3) DuPont Zonyl. *Fluorochemical Intermediates*, 2001.
(4) Krafft, M. P. *Curr. Opin. Colloid Interface Sci.* **2003**, *8*, 213.
(5) Beckman, E. J. *J. Supercrit. Fluids* **2004**, *28*, 121.
(6) Kendall, J. L.; Canelas, D. A.; Young, J. L.; DeSimone, J. M. *Chem. Rev.* **1999**, *99*, 543.
(7) Kirby, C. F.; McHugh, M. A. *Chem. Rev.* **1999**, *99*, 565.
(8) Tomasko, D. L.; Li, H.; Liu, D.; Han, X.; Wingert, M. J.; Lee, L. J.; Koelling, K. W. *Ind. Eng. Chem. Res.* **2003**, *42*, 6431.
(9) Jackson, G.; Chapman, W. G.; Gubbins, K. E. *Mol. Phys*. **1988**, *65*, 1.
(10) Chapman, W. G.; Jackson, G.; Gubbins, K. E. *Mol. Phys*. **1988**, *65*, 1057.
(11) Wertheim, M. S. *J. Chem. Phys.* **1986**, *85*, 2929.
(12) Wertheim, M. S. *J. Chem. Phys.* **1987**, *87*, 7323.
(13) Huang, S. H.; Radosz, M. *Ind. Eng. Chem. Res.* **1990**, *29*, 2284.
(14) Carnahan, N. F.; Starling, K. E. *J. Chem. Phys*. **1969**, *51*, 635.
(15) Chen, S. S.; Kreglewski, A. *Ber. Bunsen-Ges. Phys. Chem*. **1977**, *81*, 1048.
(16) Müller, E. A.; Gubbins, K. E. In *Equations of State for Fluids and Fluid Mixtures;* Sengers, J. V., Kayser, R. F., Peters, C. J., White, H. J., Jr., Eds.; Experimental Thermodynamics; Elsevier: Amsterdam, 2000; Vol. 5, pp 435−478.
(17) Müller, E. A.; Gubbins, K. E. *Ind. Eng. Chem. Res.* **2001**, *40*, 2193.
(18) Wei, Y. S.; Sadus, R. *AIChE J.* **2000**, *46*, 169.
(19) Economou, I. G. *Ind. Eng. Chem. Res.* **2002**, *41*, 953.
(20) Blas, F. J.; Vega, L. F. *Ind. Eng. Chem. Res.* **1998**, *37*, 660.
(21) Blas, F. J.; Vega, L. F. *J. Chem. Phys*. **1998**, *109*, 7405.
(22) Chapman, W. G. *J. Chem. Phys*. **1990**, *93*, 4299.
(23) Johnson, J. K.; Zollweg, J. A.; Gubbins, K. E. *Mol. Phys.* **1993**, *78*, 591.
(24) Dias, A. M. A.; Pamies, J. C.; Coutinho, J. A. P.; Marrucho, I. M.; Vega, L. F. *J. Phys. Chem. B* **2004**, *108*, 1450.
(25) Gross, J.; Sadoswki, G. *Ind. Eng. Chem. Res*. **2001**, *40*, 1244.
(26) Barker, J. A.; Henderson, D. *J. Chem. Phys*. **1967**, *47*, 2856.
(27) Gross, J.; Sadoswki, G. *Fluid Phase Equilb.* **2002**, *168*, 183.
(28) Gil-Villegas, A.; Galindo, A.; Whitehead, P. J.; Mills, S. L.; Jackson, G.; Burgess, A. N. *J. Chem. Phys.* **1997**, *106*, 4168.
(29) Galindo, A.; Davies, L. A.; Gil-Villegas, A.; Jackson, G. *Mol. Phys.* **1998**, *93*, 241.
(30) Galindo, A.; Gil-Villegas, A.; Jackson, G.; Burgess, A. N. *J. Phys. Chem. B* **1999**, *103*, 10272.
(31) Galindo, A.; Gil-Villegas, A.; Whitehead, P. J.; Jackson, G.; Burgess, A. N. *J. Phys. Chem. B* **1998**, *102*, 7639.
(32) McCabe, C.; Jackson, G. *Phys. Chem. Chem. Phys*. **1999**, *1*, 2057.
(33) McCabe, C.; Galindo, A.; Garcia-Lisbona, M. N.; Jackson, G. *Ind. Eng. Chem. Res*. **2001**, *40*, 3835.
(34) McCabe, C.; Galindo, A.; Gil-Villegas, A.; Jackson, G. *J. Phys. Chem. B* **1998**, *102*, 8060.
(35) Colina, C. M.; Galindo, A.; Blas, F. J.; Gubbins, K. E. *Fluid Phase Equilb.* **2004**, *222*−*223*, 77.
(36) Galindo, A.; Blas, F. J. *J. Phys. Chem. B* **2002**, *106*, 4503.
(37) Blas, F. J.; Galindo, A. *Fluid Phase Equilb.* **2002**, *194*−*197*, 501.
(38) Percus, J. K.; Yevick, G. J. *Phys Rev.* **1958**, *110*, 1.
(39) Boublik, T. *J. Chem. Phys.* **1970**, *53*, 471.
(40) Press, W. H.; Teukolsky, S. A.; Vetterling, W. T.; Flannery, B. P. *Numerical Recipes in Fortran*, 1st ed.; Cambridge University Press: Cambridge, U.K., 1986.
(41) Kreglewski, A. *Bull. Acad. Pol. Sci*. **1962**, *10*, 629.
(42) Prausnitz, J. M.; Lichtenthaler, R. N.; Gomez de Azevedo, E. *Molecular Thermodynamics of Fluid-Phase Equilibria*, 3rd ed.; Prentice Hall: Upper Saddle River, NJ, 1999.
(43) Scott, R. L.; van Konynenburg, P. H. *Discuss. Faraday Soc*. **1970**, *49*, 87.
(44) Hicks, C. P.; Young, C. L. *Chem. Rev.* **1975**, *75*, 119−175.
(45) Wallas, S. *Phase Equilibria in Chemical Engineering;* Butterworth Publishers: Boston, 1985.
(46) Francis, A. W. *J. Phys. Chem.* **1954**, *58*, 1099.
(47) Andersen, J. G.; Koak, N.; de Loos, T. W. *Fluid Phase Equilib.* **1999**, *163*, 259.
(48) Ohgaki, K.; Katayama, T. *J. Chem. Eng. Data* **1976**, *21*, 5355.
(49) Wagner, Z.; Witchterle, I. *Fluid Phase Equilib.* **1987**, *33*, 109.
(50) Li, Y.-H; Dillard, K. H.; Robinson, R. L., Jr. *J. Chem. Eng. Data* **1981**, *26*, 53.
(51) Kho, Y. W.; Conrad D. C.; Knutson, B. L. *Fluid Phase Equilib*. **2003**, *206*, 179.
(52) Iezzi, A.; Bendale, P.; Enick, R.; Turberg, M.; Brandy, J. *Fluid Phase Equilib*. **1989**, *52*, 307.
(53) Duce, C.; Tine, M. R.; Lepori, L.; Matteoli, E. *Fluid Phase Equilib.* **2002**, *199*, 197.
(54) Gaw, W. J.; Scott, R. L. *J. Chem. Thermodyn*. **1971**, *3*, 335.
(55) Dunlap, R. D.; Bedford, R. G.; Woodbrey, J. C.; Furrow, S. D. *J. Am. Chem. Soc.* **1959**, *81*, 2927.
(56) Hicks, C. P.; Hurle, R. L.; Toczylkin, L. S.; Young, C. L. *Aust. J. Chem*. **1978**, *31*, 19.
(57) Bondar, V. Personal Communication, 2003.
(58) Zhang, L.; Siepmann, J. I. *J. Phys. Chem. B* 2004, in press.
(59) Christou, G.; Morrow, T.; Sadus, R. J.; Young, C. L. *Fluid Phase Equilb*. **1986**, *25*, 263.